Supplementary Information: A solid-state NMR and DFT Study of Compositional Modulations in $Al_xGa_{1-x}As$

Paulus J. Knijn, P. Jan M. van Bentum, Ernst R.H. van Eck,
Changming Fang, Dennis L.A.G. Grimminck, Robert A. de Groot,
Remco W.A. Havenith, Martijn Marsman, W. Leo Meerts,
Gilles A. de Wijs and Arno P.M. Kentgens

This supplementary is divided into an experimental NMR section, concerning the QCPMG data and a theoretical DFT part.

1 Experimental

Due to the huge breadth of the arsenic spectrum, even at 18.8 T, high rf fields are advantageous since they can excite the entire spectrum. Besides the strength of the rf field, special attention is given to the homogeneity over a wide frequency range. To this end a series of reference experiments were performed by measuring the ^{75}As nutation of a reference GaAs sample with 820 Watt power.

1.1 Effective rf field strength

The rf field intensity was 520 kHz and reduced only 7.5% -1.5 MHz away from its tuned resonance frequency, see Fig. 1. To obtain the strong rf fields, we need high power levels. However, at these powers, the build-up and decay time of the pulse are relevant, since the pulses become relatively short. The rf field derived from nutation was 520 kHz, however, this nutation frequency was derived from the nutation spectrum, including pulses with a length of 20 μs. At short times, the energy applied to the probe will take some time to build-up and decay. Consequently, the effective rf field is reduced. For a resonant circuit with a Q of $\sim$20, the build-up/decay time is $\tau_b \approx$ 0.15 μs. The energy build-up in the circuit as a function of time can be described with $P(t) = P_{max} \cdot (1 - e^{-t/\tau_b})$. The rf field scales with the square root of the applied power $\nu_{rf} \propto \sqrt{P}$. We derive $\nu_{rf}(t) = \nu_{rf}^{max} \cdot \sqrt{1 - e^{-t/\tau_b}}$. Substituting $\nu_{rf}^{max} = 520$ kHz from the nutation, the RF field at $t = 0.32$ μs reduces to $\approx$488 kHz, see left figure of Fig. 2. We applied a frequency-stepped QCPMG to the two $Al_xGa_{1-x}As$ samples. The QCPMG pulse sequence is displayed on the right side of Fig. 2.

1.2 QCPMG Analysis

The center frequency ^{75}As QCPMG signal of $x \sim 0.489$ was first simulated. The simulated signals from the echo train were added and it was verified that the relative echo intensity from the two central sites, $n = 0, 4$ dropped to $\approx 60\%$ at the 242^{th} echo, while the $n = 1, 2, 3$ sites refocused almost for 100 %. The quadrupolar coupling from both sites is very different, thus it is not possible to refocus all sites and the 180 degree echo mostly selectively focusses the intensity from the $n = 1, 2, 3$ sites.

In five simulations we determined the theoretical T_2 projection decays solely due to quadrupolar evolution. This decay fitted reasonably to a single exponent, for $n = 0, 1, 2, 3, 4$ we derived 16.4, 20.8, 12.9, 20.8, 25.0 ms. Experimentally the decay was stronger $\sim$ 8 ms, see Fig. 3.

Now we consider the off-resonance behavior. In the SIMPSON simulations, we simulated one whole-echo for all the sites and all the off-resonance frequencies ($\frac{\pi}{2}^y$-τ_s-$\tau_{acq}/2$-π^x-τ_s-ACQ^x), with selective pulse times and the delay time $\tau_s = \tau - \tau_{acq}/2 - t_{90}$. I_{1m} was used as detection operator and the -1 coherence was filtered out after the 90 and 180 degree pulse. The off-resonance, single echo spectra were simulated using $\eta = 1$, $C_q = 610/820$ kHz for $n = 0, 4$ and $\eta = 0.06/0.94$, $C_q = 33.4$ MHz for $n = 1, 2, 3$. The latter sites were broadened by convolution with a Gaussian function. In agreement with our expectations considering the reduced rf field due to the short pulse times, the fits of each frequency significantly improved when the simulated RF field was reduced from 520 kHz

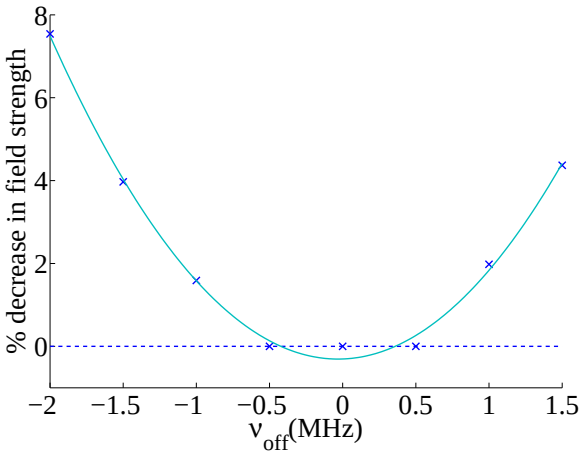

Figure 1: A series of reference experiments were performed by measuring the arsenic nutation of GaAs with 820 Watt power at different frequency offsets. The profile confirms the Q factor of the probe of ∼20. The maximum rf field strength was 520 kHz.

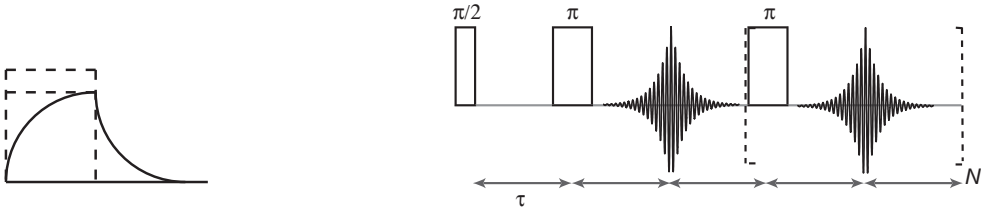

Figure 2: (left) Experimental pulse time build-up and decay. (right) Frequency-stepped-whole-echo QCPMG on ^{75}As, echo time = τ = 140 μs , τ_{acq} = 125 μs, 500 points per echo and 242 echoes, $\pi/2$ = 0.32 μs, π = 0.62 μs, ν_{rf} = 520 kHz, power = 800 Watt, spectral width = 4 MHz, frequency step size was 125 kHz. The pulse delay was 1 second. More experimental settings are tabulated in Table 1.

(nutation) to 455 kHz (the effective rf field). The corresponding simulated, effective pulse times were 0.27 and 0.54 μs. The effective rf field of 455 kHz is close to the predicted 488 kHz, on the basis of the pulse build-up time.

The fits of the $x \approx 0.489$ spectra are displayed in Figure 4. Clearly, the shape and relative intensities of the spectra are affected by the quadrupolar distribution, the off-resonance frequency, the T_2's and the echo train. The central and satellite intensities have to be considered to calculated the relative intensities. Here, they are incorporated in the SIMPSON output.

In Fig. 5 the fitted relative intensities are plotted at different frequency offsets. It turned out that the five relative intensities were not constant but depended on the off-resonance frequency. Since only one echo is simulated, it is likely that the off-resonance evolution of the 180 degree echo-train is responsible different relative intensities per frequency. This was also hinted by the $n = 0, 4$ sites which for example had zero relative intensity around $\pm$1.0 MHz. Although, the single echo simulation was able to predict the shape and the relative intensities around the center frequency, the relative intensities far off-resonance were in disagreement with the experiment. Because the off-resonance relative intensities were not correct, we use the (close to) on-resonance data and relate the relative intensities to the order parameter S. In the figure, the solid, horizontal lines show the relative intensities for the best S_{CuAu} / S_{CuPt} and x. The best fit to the $x \approx 0.489$ data was with $S = 0$ and $x = 0.487$. This x is within the allowed 0.5% tolerance. Even if the relative intensities from five fits around the center frequency are averaged, the result is similar. For $x \approx 0.489$ we obtain a low order parameter S, in other words random arrangement of the cations.

Table 1: Settings of the frequency-stepped QCPMG. In both cases the center frequency was 136.935 MHz.

	$\mathbf{Al_{0.297}Ga_{0.703}As}$	$\mathbf{Al_{0.489}Ga_{0.511}As}$
acquisitions	10.000	5.400
number of frequencies	24	22
freq. range (MHz)	135.310 ... 138.185	135.435 ... 138.060
	-1.625 ... 1.250	-1.500 ... 1.125

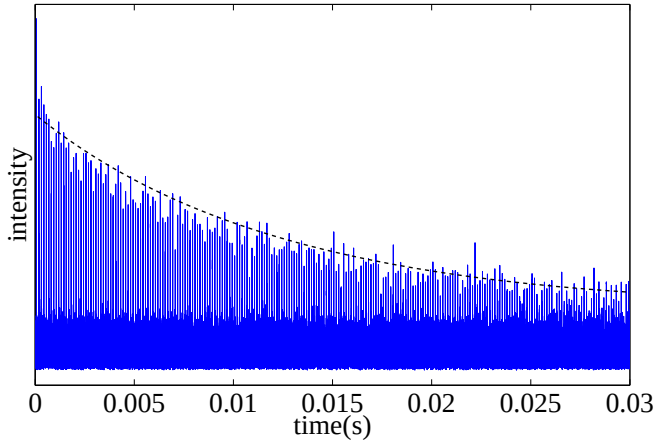

Figure 3: ^{75}As time signal of $Al_{0.489}Ga_{0.511}As$, were all 242 echoes are visible, using 5400 acquisitions. The dashed line indicates the decay of the echo train caused by the T_2^*.

2 Density Functional Calculations

This section gives (a) a brief description of the implementation of the EFG calculation in VASP [1, 2, 3, 4], (b) provides test calculations on solid state models of $Al_xGa_{1-x}As$ using VASP with various PAW projector sets, (c) provides test calculations on molecular models for $Al_xGa_{1-x}As$ using both VASP and the quantum chemical package DALTON [5], and (d) provides additional data on the "multipole model". The main objective of (b) and (c) is to estimate the influence of core states.

Similarly to pseudopotential methods, in the projector-augmented-wave PAW method [6, 7] the core electrons are frozen and removed from the electronic structure calculation. The Kohn-Sham states and the charge density are represented on a rather coarse-grained grid. Contrary to a pseudopotential method, wherein the orthogonalisation to the core states is removed, the PAW method uses an augmentation procedure to fully describe the nodal structure of Kohn-Sham states, charge density and potential. Moreover, it is possible to "unfreeze" shallow core states so that also their contribution to the EFGs can be calculated.

2.1 EFG theory & implementation

The EFG calculation was implemented following Petrilli *et al.*[8] The central quantity to be calculated is the traceless EFG tensor

$$V_{ij} = \left(\partial_i\partial_j - \frac{1}{3}\delta_{ij}\nabla^2\right) v \tag{1}$$

that is to be evaluated at each nucleus. Here i and j denote the Cartesian coordinates. In the PAW method the electrostatic potential v is a sum of three contributions:

$$v(\mathbf{r}) = \tilde{v}(\mathbf{r}) - \sum_{\mathbf{R}} \tilde{v}^1_{\mathbf{R}}(\mathbf{r}) + \sum_{\mathbf{R}} v^1_{\mathbf{R}}(\mathbf{r}) \tag{2}$$

The soft potential $\tilde{\mathbf{v}}$ is augmented within the PAW spheres centered at the nuclear sites ($\mathbf{R}$), where the soft on-site (one-center) potentials $\tilde{v}^1_{\mathbf{R}}(\mathbf{r})$ are replaced by their all-electron counterparts $v^1_{\mathbf{R}}(\mathbf{r})$.

The soft potential $\tilde{\mathbf{v}}$ is obtained via the Poisson equation from the soft charge density on the FFT grid. Its gradients are evaluated as a summation in reciprocal space at exactly the nuclear positions ($\mathbf{r} \to \mathbf{R}$). The

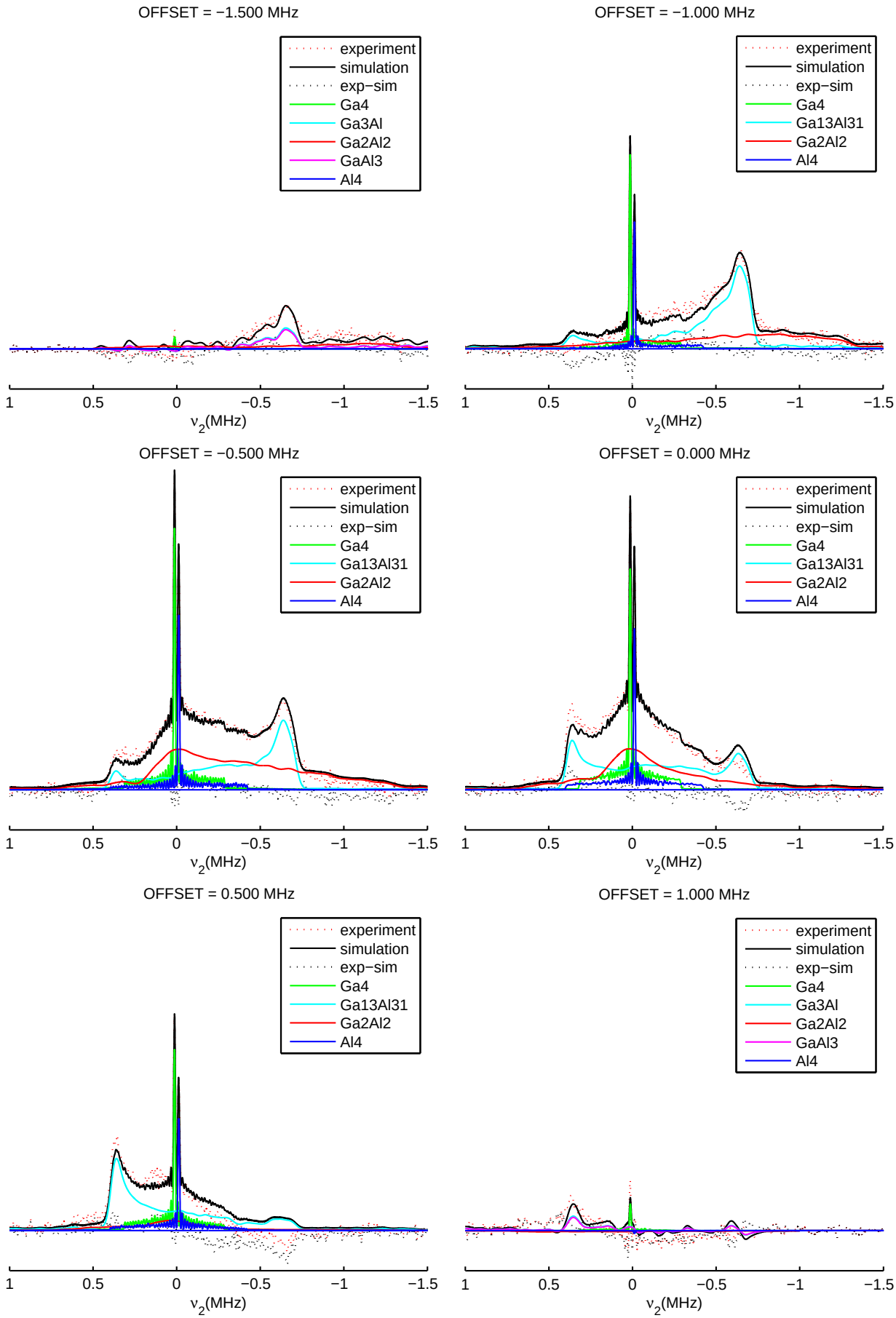

Figure 4: Off-resonance behavior of the absolute QCPMG spectra. The plotted, absolute simulated spectra were acquired using a single echo and a single quadrupolar interaction. The simulated sites with $C_q = 33.5$ MHz were broadened using a Gaussian convolution of 50 kHz for $n = 1, 3$ and 80 kHz for $n = 2$.

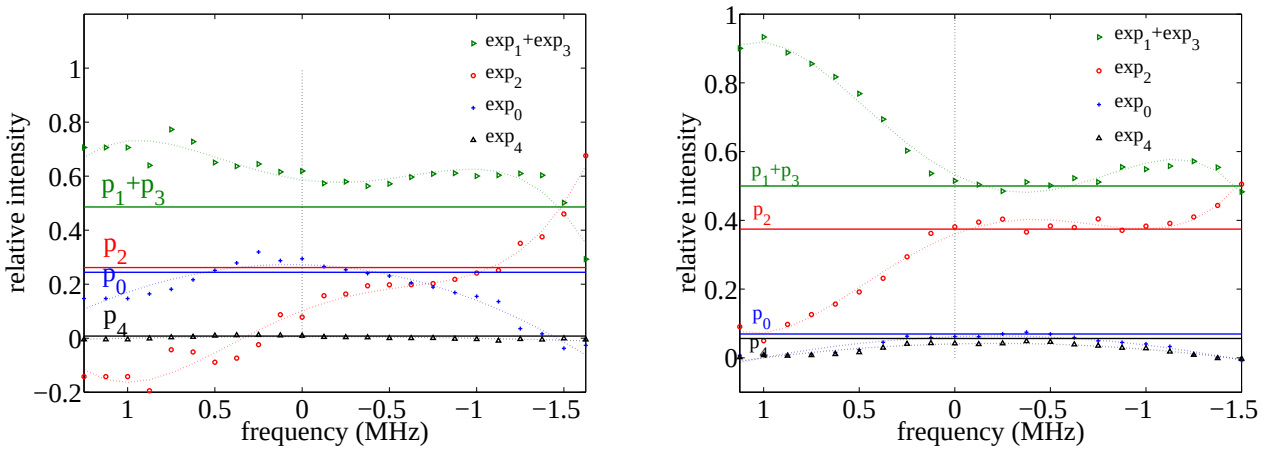

Figure 5: The data points are the relative intensities as a function of the off-resonance frequency, fitted to a second order polynomial $\exp_i$ (dotted line). The solid lines p_i are the theoretical relative intensities for $S = 0$ and $x = 0.298$ (left), $x = 0.487$ (right).

		V_{xx}	V_{yy}	V_{zz}
LAPW[a]	O	-19.6	-1.7	21.3
PAW[a]	O	-20.6	-0.8	21.4
PAW[b]	O	-17.7	-2.1	19.8
PAW[c]	O	-19.4	-1.8	21.2
LAPW[a]	Ti	14.9	6.0	-20.9
PAW[a]	Ti	13.1	7.5	-20.6
PAW[b]	Ti	15.6	7.4	-23.0
PAW[c]	Ti	14.8	6.5	-21.3

Table 2: Rutile TiO_2 EFG components (V/Å^2). Cell and positional parameters are from Ref. [8], Table III. All PAW calculations: Ti $3s$ and $3p$ treated as valence electrons. LAPW[a] & PAW[a], Petrilli *et al.* [8]; PAW[b], VASP standard potentials; PAW[c], VASP optimized potentials.

contribution from the ionic nuclei is absorbed into the soft charge density as Gaussians centered at the atomic positions.

Both on-site terms $\tilde{v}^1_{\mathbf{R}}$ and $v^1_{\mathbf{R}}$ consist of radial functions represented on a logarithmic grid multiplied by real spherical harmonics Y_L:

$$v^1_{\mathbf{R}}(\mathbf{r}) = \sum_L v^1_{\mathbf{R},L}(|\mathbf{r}-\mathbf{R}|)Y_L(\widehat{\mathbf{r}-\mathbf{R}}) \tag{3}$$

Only the terms with angular momentum $l = 2$ contribute to the EFG and require evaluation of quantities $v^1_{\mathbf{R},L}(|\mathbf{r}-\mathbf{R}|)/|\mathbf{r}-\mathbf{R}|^2$ in the limit $|\mathbf{r}-\mathbf{R}| \to 0$. These are obtained by extrapolation from the first grid points of the logarithmic mesh. More detail on the method can be found in the paper by Petrilli *et al.*[8] that we closely follow.

Several test calculations were carried on various molecular and solid state systems. Here we just report some of the calculations on TiO_2 in Table 2. We use the same geometry as Petrilli *et al.* Ti $3s$ and $3p$ states were treated as semi-core states. Standard PAW Potentials as supplied with the VASP package were used, as well as highly optimized very accurate projector sets. The calculations were carried out in the LDA.

2.2 Convergence tests on ordered Al_xGa_yAs crystals

Several convergence tests were carried out, most of them using the LDA, in particular to estimate the effect of the semi-core states. We used a tetragonal and cubic cells with compositions $AlGaAs_2$, $AlGa_3As_4$ and Al_3GaAs_4. This allows to test with various As first coordination shells: 2 Al and 2 Ga in case of $AlGaAs_2$, 1 Al and 3 Ga in case of $AlGa_3As_4$ and 3 Al and 1 Ga in case of Al_3GaAs_4. The lattice constant was $a = 5.6394$ Å and atoms were kept fixed at their positions on an idealized zincblende lattice. Results are summarized in tables 3, 4 and 5.

			V_{zz} (V/Å^2)			η
Al	Ga	As	Al	Ga	As	As
		LDA				
[Ne]	[Ar]3d^{10}	[Ar]3d^{10}	0.13	-0.67	-48.1	0.93
[Ne]	[Ar]	[Ar]3d^{10}	0.14	-0.63	-50.0	0.92
1s^{2}2s^2	[Ar]	[Ar]3d^{10}	0.032	-0.63	-50.0	0.92
[Ne]	[Ar]	[Ar]	0.14	-0.62	-50.0	0.92
[Ne]	[Ar]	[Ar]*	0.14	-0.62	-49.6	0.92
[Ne]	[Ne]3s^2	[Ar]3d^{10}	0.14	-0.45	-50.0	0.92
1s^{2}2s^2	[Ne]3s^2	[Ar]	0.031	-0.44	-50.0	0.92
		GGA				
[Ne]	[Ar]	[Ar]3d^{10}	0.11	-0.50	-45.4	0.93
[Ne]†	[Ar]	[Ar]3d^{10}	0.13	-0.46	-45.3	0.93

Table 3: Electric field gradients V_{zz} and asymmetry parameters η calculated with various projector sets for $AlGaAs_2$. The frozen core states are listed. *As_d_GW. †Al_h (used for the calculations).

			V_{zz} (V/Å^2)	
Al	Ga	As	Ga	As
		LDA		
[Ne]	[Ar]3d^{10}	[Ar]3d^{10}	0.63	-46.7
[Ne]	[Ar]	[Ar]3d^{10}	0.54	-48.5
1s^{2}2s^2	[Ar]	[Ar]3d^{10}	0.54	-48.4
[Ne]	[Ar]	[Ar]	0.54	-48.4
[Ne]	[Ne]3s^2	[Ar]3d^{10}	0.27	-48.5
1s^{2}2s^2	[Ne]3s^2	[Ar]	0.33	-48.4
		GGA		
[Ne]	[Ar]	[Ar]3d^{10}	0.43	-44.2

Table 4: Electric field gradients V_{zz} calculated with various projector sets for $AlGa_3As_4$. The frozen core states are listed. $V_{zz,Al} = 0$, $\eta_{Ga} = \eta_{As} = 0$.

The test results show that the Ga 3d states cannot be kept in the frozen core, but need to be treated as valence. They do not only affect the Ga EFG but also the As EFG. The Ga 3p states also have a substantial effect on the small Ga EFG. The effect of the 3p states, that are 90 eV below the valence band edge, on the Ga EFG is considerably larger (∼30 %) than the effect of the shallow Ga 3d core states (∼6 %). For Al the 2p core states also give rise to a large relative effect: unfreezing the 2p states (about 60 eV below the valence band edge) reduces the small Al EFG by roughly a factor 2 in $AlGaAs_2$ and 4 in Al_3GaAs_4. For $AlGa_3As_4$ their relaxation even has a small effect on the Ga EFG. The effect of the arsenic 3d states is rather small: although in an absolute sense it is comparable to the core effects of Al and Ga, it only changes the arsenic EFG by one percent.

In the PAW method it is difficult to include core states deeper than those considered above. It requires good scattering over such a wide energy range, hence inclusion of many projector functions, that ghost states start to occur. In order to asses the effect of the frozen core approximation, molecular calculations were performed of small model systems, comparing the PAW method and all-electron results obtained with a quantum chemical package.

2.3 Molecular calculations on small model systems for $Al_xGa_{(1-x)}As$

To assess the effect of the frozen core approximation in the solid state calculations described earlier, molecular calculations were performed on small model systems for $Al_xGa_{(1-x)}As$ (Figure 6). Model system **m1** mimics the environment of the As atom in the solid state, **m2** that of Al, and **m3** that of the Ga atom. The Al, Ga, and As positions in these model systems occupy the positions these atoms have in the crystal structure, and only the positions of the pseudo-hydrogen atoms (see Fig. 6) have been optimized. The basis set used in the calculations of the electric field gradient was the cc-pVTZ basis set, but all functions were un-contracted. The calculations were performed using the LDA functional with DALTON [5]. Scalar relativistic effects were treated using the Douglas-Kroll formalism.[1] The calculations were also performed with VASP at the LDA level, using potentials where the

[1] The effect of the so-called picture change [9] was neglected. For our nuclei this is still a good approximation.

			V_{zz} (V/Å^2)	
Al	Ga	As	Al	As
		LDA		
[Ne]	[Ar]	[Ar]3d^{10}	-0.17	49.5
1s^{2}2s^2	[Ar]	[Ar]3d^{10}	-0.085	49.4

Table 5: Electric field gradients V_{zz} calculated with various projector sets for Al_3GaAs_4. The frozen core states are listed. $V_{zz,Ga} = 0$, $\eta_{Al} = \eta_{\mathrm{As}} = 0$.

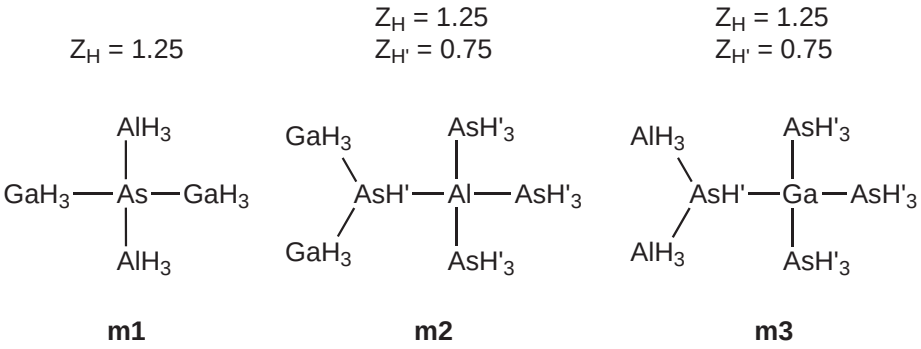

Figure 6: Model systems for $Al_xGa_{(1-x)}As$. The nuclear charges of the pseudo-hydrogen atoms (H and H′) are denoted by Z_H and $Z_{H'}$, respectively.

3d electrons for As and Ga and the 2p electrons for Al were taken into account, while the other lower-lying orbitals were treated as frozen core ([Ar] core for Ga and As and a 1s^{2}2s^2 core for Al).

In DALTON, the EFG tensor is calculated as an expectation value $V_{\alpha\beta} = \langle\psi|\hat{V}_{\alpha\beta}|\psi\rangle$, with α, β the carthesian components of interest. Thus, the EFG tensor is a sum of (occupied) orbital (ϕ) contributions: $V_{\alpha\beta} = \sum_i^{N/2}\langle\phi_i|\hat{V}_{\alpha\beta}|\phi_i\rangle$ (N is the number of electrons). Note that these orbital contributions do not have any direct physical meaning, but that the contribution of the core orbitals to this expectation value of V is an indication of the error introduced by the frozen core approximation. In Table 6 the calculated V_{zz} component for the nucleus of interest for the three model compounds is shown, together with its core contribution. The non-diagonal form of the EFG tensor for Al and Ga in **m2** and **m3**, respectively, thwarts the simple decomposition in orbital contributions to V_{zz}. Therefore, the core contribution to the EFG tensor for these compounds is obtained by subtracting the core contributions to all tensor components before diagonalisation. The difference between the largest eigenvalues of the total EFG tensor and this non-core EFG tensor is taken as the core contribution to V_{zz}.

The relative deviations between the VASP and full-molecular results are 3.2% (As), 3.8% (Al) and 2.5% (Ga). Upon application of this ad-hoc core-correction, the relative deviations in V_{zz} values reduce to 0.03% for As, and to 0.3% for Ga. The 1s and 2s Al-core orbitals do not significantly contribute to the V_{zz} value, and the core-correction even deteriorates the agreement between VASP and the full-molecular results. Differences between VASP and DALTON are not only due to the neglect of core relaxation in the former type of calculations; small differences are also expected because of differences in basis set (plane waves *vs.* atomic centered Gaussians) and a different treatment of relativistic effects. Still, these calculations provide evidence that core contributions can be significant for As (3.7%) and Ga (2.1%). Hence, EFG calculations using the frozen core approximation are not expected to be more accurate than *ca.* 5%.

2.4 Core states: conclusion

With the calculations on the molecular models we could test the effect of those core states that are too deep be included (i.e. to unfreeze) in the PAW approach. The effects are small. We have to be careful though: Whereas the arsenic V_{zz} attains values typical for the solid state environment, the asymmetry necessarily present in these molecular models gives rise to much larger Ga and Al V_{zz} than we observe in the solid state. In the typical solid state environment, these EFGs are one to two orders of magnitude smaller, and are determined by weak long-range effects. Moreover, from the solid state model calculations we know that, e.g, the 2p electrons in Al can have substantial *relative* effects: suppressing the 2p will only marginally change the absolute size of the EFGs, this small

MO	As-V_{zz} in **m1**	Al-V_{zz} in **m2**	Ga-V_{zz} in **m3**
Core[a]	-1.701	-0.004	-0.366
Total - core	-52.493	4.261	-16.836
Total	-54.194	4.257	-17.202
VASP	-52.478	4.103	-16.782

Table 6: The V_{zz} components and core/valence contributions (in V/Å^2) to V_{zz} for the As atom of **m1**, the Al atom of **m2**, and the Ga atom of **m3**. [a]The core orbitals are 1s, 2s, 2p, 3s, and 3p for As and Ga, and 1s and 2s for Al.

	Sea of Al	Sea of Ga
$n = 0$ and $n = 4$		
$\langle\eta\rangle$	0.61	0.61
$\langle V_{zz}\rangle$	1.19	0.98
$n = 1$ and $n = 3$		
$\langle\eta\rangle$	0.03	0.03
$\langle V_{zz}\rangle$	43.6	43.2
$n = 2$		
$\langle\eta\rangle$	0.98	0.98
$\langle V_{zz}\rangle$	43.8	43.4

Table 7: Comparison of the average values for $S = 0$ obtained with the "multipole model" based on DFT calculations for $Al_{255}GaAs_{256}$ ("sea of Al") and for $AlGa_{255}As_{256}$ ("sea of Ga"). V_{zz} is in units of 10^{-20} V/m^2. The Gallium sea returns slightly lower EFG values.

change is however more than 50 % of the total Al EFG (Table 3).

For reasons of computational efficiency (calculations on large cells of up to 512 atoms have to be carried out) we chose to employ standard PAW projector sets, as are supplied with the VASP package. These allow for a kinetic energy cutoff of 300 eV (500 eV for the augmentation grid). So the full Al core is frozen, all Ga electrons below 3d are frozen and even the 3d of arsenic remains frozen. For Al we expect large errors. For Ga the situation is much better, but inaccuracies of several 10 % are possible. For arsenic the expected inaccuracies are modest, no more than 5 % for As sites with large EFGs. Somewhat larger inaccuracies are expected for As[Al_4] and As[Ga_4] sites.

2.5 Choice of DFT functional

The choice of DFT functional has a noticeable effect. Using standard LDA (Perdew-Zunger parametrization of the Cerperley Alder correlation energy of the uniform electron gas) or the Perdew-Burke-Ernzerhof (PBE, Ref. [10]) generalized gradient approximation (GGA) gives a difference of 9 % for the As V_{zz} (see Table 3). This is larger than possible systematic errors resulting from neglect of core-relaxation.

Many studies on EFGs in solids have been carried out using the LDA. Very good results can be obtained. Systematic studies of the effect of exchange-correlation functionals on the EFG in solids have, to our knowledge, not been carried out. More accurate studies beyond DFT methods are not available. In this study we use the state-of-the-art PBE functional for our calculations. It gives good agreement with the experiment.

2.6 Multipole model

Table 7 provides info on the effect of using the "Ga in a sea of Al" or the "Al in a sea of Ga" on the As EFGs.

A Simpson files

A.1 Hahn-echo script

```
spinsys {
   channels 75As
   nuclei   75As
   quadrupole 1 2 1e6 0.1 0 0 0
}

par {
   proton_frequency  800e6
   sw                5000000.0
   np                4000
   ni                1
   crystal_file      $crystal_file
   gamma_angles      1
   start_operator    I1z
   detect_operator   I1p
   verbose           1111
   variable dw       1000000.0/sw
   variable t_acq    np*dw
   variable tau1     200         #al3ga7, 175us for al5ga5
   variable tau2     100         #al3ga7, 25us  for al5ga5
   variable rf       625000
   variable t90      0.125e6/rf  #sel. pulse I=3/2 (75As) 0.2us exp.
   variable t180     0.25e6/rf   #0.4us exp.
}

proc pulseq {} {
  global par
  #prop 1 - for acq
  reset
  delay  $par(dw)
  store 1

  #actual pulse program
  reset
  pulse $par(t90) $par(rf) [lindex {x -x} $par(p)]
  delay $par(tau1)
  pulse $par(t180) $par(rf) [lindex {-y -y} $par(p)]
  delay $par(tau2)
  acq $par(np) 1 [lindex {x -x} $par(p)]
}

proc main {} {
  global par
  foreach site {0 1 2} {
   if {$site==0} {
      # central + sattelites
      for {set par(etaT) 0} {$par(etaT)<=100} {incr par(etaT) 5} {
         for {set par(Qcc) 0} {$par(Qcc)<=1400000} {incr par(Qcc) 200000} {
            set par(eta) [expr $par(etaT)/100.0]
            set par(name) A
            set par(crystal_file) zcw4180
            set par(detect_operator) I1p
            run
         }
      }
   }
   if {$site==1} {
      # central transition
      for {set par(etaT) 0} {$par(etaT)<=10} {incr par(etaT) 1} {
         for {set par(Qcc) 31000000} {$par(Qcc)<=35000000} {incr par(Qcc) 100000} {
            set par(eta) [expr $par(etaT)/100.0]
            set par(name) B
            set par(crystal_file) zcw28656
            set par(detect_operator) I1c
            run
         }
      }
   }
   if {$site==2} {
      # central transition, eta 1 is assymetic -> more orientations needed!!
      for {set par(etaT) 92} {$par(etaT)<=100} {incr par(etaT) 1} {
         for {set par(Qcc) 31000000} {$par(Qcc)<=35000000} {incr par(Qcc) 100000} {
            set par(eta) [expr $par(etaT)/100.0]
            set par(name) C
            set par(crystal_file) zcw28656
            set par(detect_operator) I1c
            run
         }
      }
```

```
   }
  }
}

proc run {} {
   global par
   set interactions [list \
      "quadrupole_1_aniso $par(Qcc)" \
      "quadrupole_1_eta $par(eta)" ]
   # 2step phase-cycling
   for {set par(p) 0} {$par(p) <2} {incr par(p)} {
      set f [fsimpson $interactions]
      if [info exist g] {
         fadd $g $f
      } else {
         set g [fdup $f]
      }
      funload $f
   }
   if {$par(name) == "A"} {
      set naam [format "%s-%1.2f-%010.1f.fid" A [expr $par(eta)] [expr $par(Qcc)]]
      fsave $g $naam
   }
   if {$par(name) == "B"} {
      set naam [format "%s-%1.2f-%010.1f.fid" B [expr $par(eta)] [expr $par(Qcc)]]
      fsave $g $naam
   }
   if {$par(name) == "C"} {
      set naam [format "%s-%1.2f-%010.1f.fid" C [expr $par(eta)] [expr $par(Qcc)]]
      fsave $g $naam
   }
   funload $g
}
```

A.2 QCPMG script

```
spinsys {
   channels 75As
   nuclei   75As
   quadrupole 1 2 1e6 0.1 0 0 0
}

par {
   proton_frequency   800e6
   sw                 4000000.0
   np                 500
   ni                 1
   crystal_file       $crystal_file
   gamma_angles       1
   start_operator     I1x
   detect_operator    I1p
   verbose            1111
   variable dw        1000000.0/sw
   variable t_acq     np*dw
   variable t_halfacq t_acq/2.0
}

proc pulseq {} {
  global par
  reset
  delay  $par(dw)
  store 1

  reset
  acq $par(np) 1 x
}

proc main {} {
  global par
  foreach site {0 1 2} {
   if {$site==0} {
      for {set par(etaT) 0} {$par(etaT)<=100} {incr par(etaT) 10} {
         for {set par(Qcc) 0} {$par(Qcc)<=2000000} {incr par(Qcc) 200000} {
            set par(eta) [expr $par(etaT)/100.0]
            set par(name) A
            set par(crystal_file) zcw4180
            run
         }
      }
   }
   if {$site==1} {
      for {set par(etaT) 0} {$par(etaT)<=10} {incr par(etaT) 1} {
         for {set par(Qcc) 31000000} {$par(Qcc)<=35000000} {incr par(Qcc) 100000} {
```

```
            set par(eta) [expr $par(etaT)/100.0]
            set par(name) B
            set par(crystal_file) zcw28656
            run
         }
      }
   }
   if {$site==2} {
      for {set par(etaT) 90} {$par(etaT)<=100} {incr par(etaT) 1} {
         for {set par(Qcc) 31000000} {$par(Qcc)<=35000000} {incr par(Qcc) 100000} {
            set par(eta) [expr $par(etaT)/100.0]
            set par(name) C
            set par(crystal_file) zcw28656
            run
         }
      }
   }
  }
}

proc run {} {
   global par
   set interactions [list \
      "quadrupole_1_aniso $par(Qcc)" \
      "quadrupole_1_eta $par(eta)" ]
   set f [fsimpson $interactions]
   if {$par(name) == "A"} {
      set naam [format "%s-%1.2f-%010.1f.fid" A [expr $par(eta)] [expr $par(Qcc)]]
      fsave $f $naam
   }
   if {$par(name) == "B"} {
      set naam [format "%s-%1.2f-%10.1f.fid" B [expr $par(eta)] [expr $par(Qcc)]]
      fsave $f $naam
   }
   if {$par(name) == "C"} {
      set naam [format "%s-%1.2f-%10.1f.fid" C [expr $par(eta)] [expr $par(Qcc)]]
      fsave $f $naam
   }
   funload $f
}
```

References

[1] G. Kresse and J. Hafner. Ab initio molecular dynamics for liquid metals. *Phys. Rev. B*, 47:558, 1993.

[2] G. Kresse and J. Hafner. Ab initio molecular-dynamics simulation of the liquid-metal amorphous-semiconductor transition in germanium. *Phys. Rev. B*, 49:14251, 1994.

[3] G. Kresse and Furthmüller J. Efficiency of ab-initio total energy calculations for metals and semiconductors using a plane-wave basis set. *Comput. Mater. Sci.*, 6:15, 1996.

[4] G. Kresse and Furthmüller J. Efficient iterative schemes for ab initio total-energy calculations using a plane-wave basis set. *Phys. Rev. B*, 54:11169, 1996.

[5] DALTON, a molecular electronic structure program, Release 2.0 (2005), see http://www.kjemi.uio.no/software/dalton/dalton.html.

[6] P.E. Blöchl. Projector augmented-wave method. *Phys. Rev. B*, 50:17953, 1994.

[7] G. Kresse and D. Joubert. From ultrasoft pseudo potentials to the projector augmented-wave method. *Phys. Rev. B*, 59:1758, 1999.

[8] H.M. Petrilli, P.E. Blöchl, P. Blaha, and K. Schwarz. Electric-field-gradient calculations using the projector augmented wave method. *Phys. Rev. B*, 57:14690, 1998.

[9] V. Kellö and Sadley A.J. Picture change and calculations of expectation values in approximate relativistic theories. *Int. J. Quant. Chem.*, 68:159–174, 1998.

[10] J.P. Perdew, K. Burke, and M. Ernzerhof. *Phys. Rev. Lett.*, 77:3865, 1996.